Water Research 247 (2023) 120744

Contents lists available at ScienceDirect

Water Research

journal homepage: www.elsevier.com/locate/watres

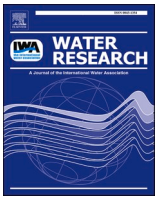

Unexpected shifts of dissolved carbon biogeochemistry caused by anthropogenic disturbances in karst rivers

Maofei Ni [a], Rui Liu [b,d], Weijun Luo [c], Junbing Pu [b,e], Jing Zhang [b,d,*], Xiaodan Wang [a]

[a] College of Eco-Environmental Engineering, Guizhou Minzu University, Guiyang 550025, China
[b] College of Geography and Tourism, Chongqing Normal University, Chongqing 401331, China
[c] State Key Laboratory of Environmental Geochemistry, Institute of Geochemistry, Chinese Academy of Sciences, Guiyang, 550081, China
[d] The Key Laboratory of GIS Application Research, Chongqing Normal University, Chongqing 401331, China
[e] Chongqing Key Laboratory of Wetland Science Research of the Upper Reaches of the Yangtze River, School of Geography and Tourism, Chongqing Normal University, Chongqing 401331, China

ARTICLE INFO

Keywords:
Carbon turnover
Anthropogenic disturbances
Biological carbon pump
CO_2 outgassing
Aquatic metabolism

ABSTRACT

Dissolved carbon (C) provides critical feedbacks to regional biogeochemical processes and global C cycling. Yet to date, the specific pathways of fluvial dissolved C turnover, particularly with human-induced shifts involved, are still poorly understood. Here, we examined dissolved inorganic (DIC) and organic C (DOC), as well as human disturbances i.e., river damming and land use in karst rivers. We show that anthropogenic activities caused unexpected shifts to dissolved C biogeochemistry. Specifically, we found that human disturbances accelerated aquatic metabolism, ultimately causing more river CO_2 generation than fixation. The extended hydrological retention by damming greatly stimulated biological utilization of dissolved C. River DOC was sourced largely from farmland and forest, while land-use fragmentation increased DOC diversity. Artificial dams and land uses intensified the transformations between DIC and DOC within karst environments. Based on these findings, we provided a process-based conceptual model regarding the rapid cycle of active C in karst waters, revealing the associated trajectories of DIC and DOC biogeochemistry. This study suggests that reducing anthropogenic disturbances essentially decelerates organic C metabolism, and therefore promotes riverine CO_2 sequestration in the context of global C neutrality.

1. Introduction

Rivers and streams receive the bulk of carbon (C) from terrestrial environments, sustaining dissolved C transport *via* lateral and vertical diffusion (Battin et al., 2023; Chen et al., 2021a; Liu et al., 2022). In fluvial systems, dissolved inorganic C (DIC) is ultimately sourced from chemical weathering of minerals and atmospheric CO_2 (Raymond and Hamilton, 2018; Zhong et al., 2020, 2023), and dissolved organic C (DOC) can arise from soil leaching and biological metabolism (Lapierre et al., 2013; Lynch et al., 2019). Consequently, dissolved C origins are highly controlled by watershed climate, lithology, and hydrology (Horgby et al., 2019; Hotchkiss et al., 2018; Longworth et al., 2007). As a critical component of aquatic C balance, dissolved C along with a major gaseous form i.e., carbon dioxide (CO_2), in turn provides feedbacks to fluvial water chemistry and biology (Campeau et al., 2017). Anthropogenic stress on fluvial C turnover, however, is poorly constrained despite the profound influence on DIC and DOC biogeochemistry (Drake et al., 2020).

Previous studies declared that human disturbances have significantly changed riverine C export, emission and sequestration (Butman et al., 2015; Raymond et al., 2008; Wohl et al., 2017). Yet to date, explicit demonstrations of the biogeochemical pathways caused by anthropogenic activities are still restricted, particularly for intricate DIC and DOC turnover in aquatic ecosystems. Growing evidence suggests that human-induced changes actively mediate dissolved C dynamics in rivers (Peng et al., 2014; Tang et al., 2021). For instance, the damming of rivers, an artificial impoundment, has made alterations to watershed hydrology, water environment and downstream ecology, as well as biogeochemical cycles of aquatic C (Li et al., 2021; Palmer and Ruhi, 2019). In this context, global river DIC and DOC can be greatly modulated by damming, given that 63 % of the world's large rivers are non-free-flowing (Grill et al., 2019).

* Corresponding author at: Chongqing Normal University (CQNU), University Town, Shapingba District, Chongqing 401331, China.
E-mail address: zhangjing@cqnu.edu.cn (J. Zhang).

https://doi.org/10.1016/j.watres.2023.120744
Received 11 July 2023; Received in revised form 10 October 2023; Accepted 15 October 2023
Available online 16 October 2023
0043-1354/© 2023 Elsevier Ltd. All rights reserved.

Land use and landscape metrics can elucidate human-induced disturbances on aquatic C evolution (Battin et al., 2009; Coble et al., 2022; Mahowald et al., 2017). The prevailing view suggests that agriculture and urbanization likely increase structural complexity of fluvial organic and inorganic C (Nai et al., 2023; Wilson and Xenopoulos, 2009; Zhao et al., 2015). Landscape metrics e.g., patch density (PD), largest patch index (LPI) and Shannon's diversity index (SHDI) are proposed to quantitatively characterize land use structures and spatial configuration, assuming to be an available predictor for human feedbacks to watershed biochemistry (Zhang et al., 2019). Prior findings reported that landscape controls hydrological export of DOC and DIC (Dornblaser and Striegl, 2015; Williamson et al., 2023). However, compositional variability and interactivity of dissolved C in rivers are largely omitted, despite their fundamental roles of aquatic C cycles.

In this study, we conducted a comprehensive study in two karst fluvial systems, unraveling the variability of dissolved C biogeochemistry in relation to anthropogenic stress. We choose carbonate-dominated rivers attributing to the large dissolved C stocks, being driven by carbonate weathering and the known spite tical C pump" (Liu et al., 2015). Meanwhile, karst and semi-karst regions are susceptible to environmental changes due to ecological vulnerability (Butscher and Huggenberger, 2008), which may highlight the rapid response of dissolved C turnover to man-made perturbations. We thus hypothesized that human activities will alter surface water DIC and DOC dynamics, for their disturbances to biogeochemical pathways of dissolved C allocation (Vilmin et al., 2016). The objectives of this study are to: (1) examine temporal shifts of dissolved C dynamics regarding compositional variability and interactivity; and (2) reveal anthropogenic influences i.e., river damming and land use on dissolved C biogeochemistry in the karst rivers. Achieving these objectives hopes to provide a conceptual framework regarding how human activities alter aquatic environments and ultimately the fate of dissolved C.

2. Materials and methods

2.1. Study area

The rivers studied were Furong (latitude 28°0′57″–29°14′23″N;

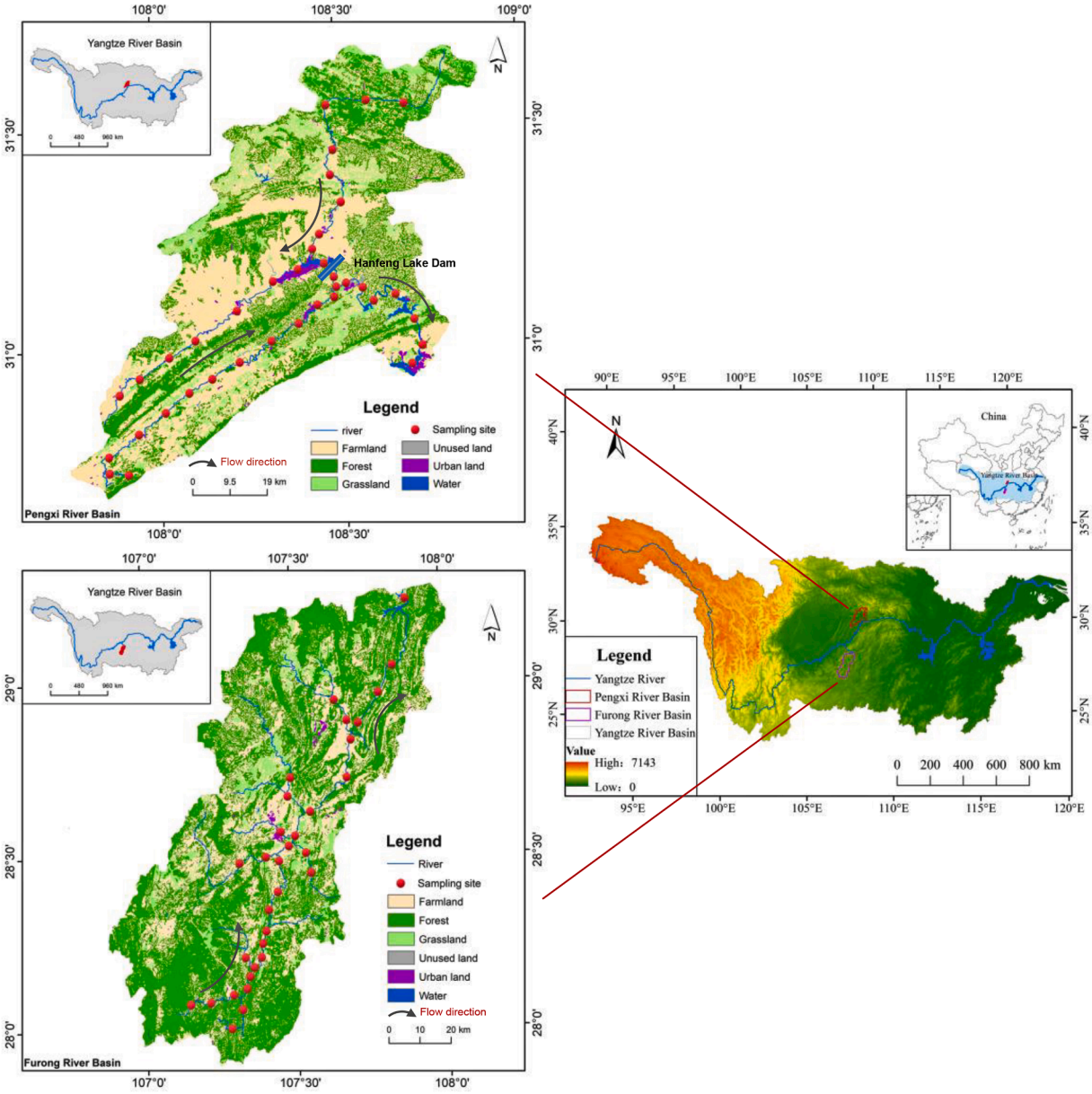

Fig. 1. Map showing sampling sites and land use in the karst rivers, China.

longitude 107°10′3″–107°52′42″E) and Pengxi (latitude 30°42′22″–31°35′22″N; longitude 107°50′49″–108°42′59″E) located respectively in the karst and semi-karst (also known as fluvial-karst) regions, Southwest China (Fig. 1). These two rivers are major tributaries of the Yangtze River with a subtropical monsoonal climate. The river Furong has a catchment area of 7406 km^2 and a total length of 231 km. Its annual rainfall and mean temperature are 1037–1233 mm (mainly concentrated in the rainy season, 86 % of the precipitation) and 16.1 °C, respectively. The discharge ranges between 15 and 58 m^3/s with an average of 34 m^3/s. Similarly, the Pengxi drains a catchment area of 5172 km^2 with a river length of 182 km. The rainfall dominantly occurs in May–September (rainy season), contributing 75 %–80 % of the annual precipitation (1100–1500 mm). The annual mean temperature varies within 10.8–18.5 °C with the highest temperature in July–August (>40 °C). River hydrology in the Pengxi is greatly regulated by water impoundment in the dry season (prolonging hydraulic retention) and flood discharge (accelerating hydraulic flow) in the rainy season. The water regulation specifically alters river discharge (17–71 m^3/s), resulting in the highest and lowest water levels in December and June, respectively. The catchment lithology is characterized by limestone, dolomite, slate, sandstone and shale in the studied rivers. Particularly, in-stream waters in the Furong and Pengxi are dominantly supplied by carbonate-dominated environments. Currently, the Furong is relatively controlled by natural conditions and thus a low human-stress river. In comparison, the Pengxi is defined as a high human-stress river due to intensive agricultural practices, urbanization and river damming (Hanfeng Lake Dam, Fig. 1).

2.2. Sample collection and measurement

Four field campaigns were performed in the rainy (July–August) and dry seasons (November–December) from 2019 to 2020, based on natural hydrological rhythm. Our samplings incorporated full spectrum of stream orders, assigning 35 and 37 sites for the river Furong and Pengxi, respectively. Briefly, a total of 137 surface waters were thus collected a depth of ~10 cm and filtered through glass microfiber filters (GF/F 47 mm, 0.7-μm, Whatman). The filtrates were kept in 100 mL high-density polyethylene (HDPE) plastic containers. The containers were sealed completely, in avoidance of any headspace or air bubbles. On-site water temperature and pH measurements were conducted with a portable CyberScan PCD 650 multi-parameters system (Eutech, USA). Current velocity was estimated using float method (5-m rope). Total alkalinity was titrated with an Alkalinity Test MColortestTM (Merck, Germany) using fixed end-point titration method. The poisoning was not arranged because of short-term transport < 48 h (Wang et al., 2021). DOC concentration and optical analyses were conducted once the refrigerated samples arrived at the laboratory.

Riverine DOC concentrations were determined using varioTOC cube/select (Elementar, Germany) and multi N/C 2100S (Analytik Jena, Germany). Under a room temperature of 25 °C, ultrapure water was used as a reference for spectroscopic measurements. UV–visible spectrum was scanned using a double-beam scanning spectrophotometer (UV-5500 PC, Shanghai), within a range of 200–700 nm (1-nm interval). Excitation-emission matrices (EEMs) were scanned using a fluorescence spectrophotometer (F-7000 FL Spectrophotometer, Japan). The excitation (Ex) and emission wavelengths (Em) were within the ranges of 200–450 nm (5-nm interval) and 250–600 nm (1-nm interval), respectively.

2.3. Land use and landscape information

The satellite images ((Landsat-8 OLI, 30 m resolution) were used to delineate land use across sampling locations. We further employed a supervised classification technique with a support vector machine algorithm by ENVI 5.1 software. Land use types were therefore divided into six categories: farm (dry land and paddy field), forest (forest and wooded areas), grass, water (rivers, reservoirs, lakes, ponds and sandy beach), urban (commercial, industrial and residential areas), and unused lands (bare ground, bare rocks and gravels). The sub-basins were identified according to previously published data in Resources and Environmental Science Data Center, CAS (http://www.resdc.cn/). Landscape metrics i.e., total area (TA), number of patches (NP), PD, LPI, edge density (ED), aggregation index (AI) and SHDI were calculated using Fragstats 4.2.1 software, reflecting land use structure and spatial configuration of landscape patterns. Consequently, we compiled compositional metrics regarding % of distinct land use categories, and quantified landscape fragmentation, dominance, structural complexity, aggregation and diversity in this study.

2.4. DIC calculations and DOC optical analysis

Riverine DIC species i.e., DIC, HCO_3^-, CO_3^{2-} and dissolved CO_2 were calculated from carbonate equilibria (water temperature, pH and total alkalinity) using CO_2SYS program (D.E. Pierrot et al., 2006). To avoid possible uncertainties from non-carbonate alkalinity, samples with pH < 5.4 were excluded in this study (Hotchkiss et al., 2015). Impetus of water-air CO_2 exchange is defined as the differences between aqueous and atmospheric partial pressure of CO_2 (ΔpCO_2, μatm). By linking to water turbulence, we modeled normalized gas transfer velocity of CO_2 (k_{600}, m/s) using an empirical model (Alin et al., 2011). River k_{600} was calibrated into site-specific gas transfer velocity (k, cm/h) using water temperature and Schmidt number. In-situ temperature and pressure were employed for Henry's constant (K_h) calibration. Because riverine CO_2 exchange was not measured directly, we calculated water-air areal CO_2 efflux (mmol/m^2/d) using thin boundary layer model as follows:

$$CO_2\ \text{efflux} = k \times K_h \times \Delta pCO_2 \quad (1)$$

For detailed information of aqueous DIC calculations and water–air CO_2 exchange estimates please see Supplementary Information S1.

Non-normalized absorption coefficient was extracted at wavelengths of 440 nm (a_{440}) to characterize UV–visible DOC composition (Naperian units). Nonlinear fit of an exponential function was used to decipher spectral slope ($S_{275–295}$) over the absorption wavelengths ranging within 275–295 nm. The ratio of absorption at 210 to 254 nm presented UV absorbance ratio index (URI). We identified fluorescent DOC composition with fluorescence regional integration, by modeling integrated intensities for five separated EEM regions (Zhou et al., 2013). EEM region I, II and IV refer to biogenic signals, expressing tyrosine- and tryptophan- and soluble microbial byproduct-like components, respectively. Region III and V are typical of bio-refractory DOC, which represent respectively fulvic acid- and humic-like components. We calculated freshness index (β:α) and humification index (HIX) as the ratios of 380 nm to 420–435 nm emission intensity at 310 nm excitation band, and 435–480 nm to 300–345 nm + 435–480 nm emission intensity at 254 nm excitation band, respectively (Hansen et al., 2016; Nai et al., 2023). Parallel factor analysis (PARAFAC) split EEM and captured collective fluorophores across samples. We selected component model and correspondence validation between excitation and emission loadings using residual analysis and split half analysis. We compared the identified fluorescence components with the open fluorescence database OpenFluor (https://openfluor.lablicate.com/), which successfully matched the observations from 109 independent studies conducted in aquatic and terrestrial environments. The maximum fluorescence intensity (F_{max}) characterized relative abundance of the corresponding PARAFAC component. For detailed information of aqueous DOC optical analysis please see Supplementary Table S1.

2.5. Quality control

We collected and analyzed the samples following the standard procedures as described in American Public Health Association (1985). The

pH probe was calibrated with 4.01, 7.00 and 9.18 pH standard solution at 25 °C, ensuring an accuracy of ±0.002 pH units. The accuracy of water temperature and uncertainty of Alkalinity Test MColortestTM were ±0.5 °C and <3 %, respectively. Previous studies indicated that non-carbonate alkalinity primarily affected to DIC chemistry and could be simply ignored in the context of non-acidic pH (Li et al., 2012; Ni et al., 2021). We estimated a maximal overestimation of 19 % for DIC species when assuming all DOC (278 μ mol/L), nitrogen (77 μmol/L) and phosphorus (1.5 μmol/L) as contributors to total alkalinity (1886 μmol/L).

Riverine DOC concentrations were determined in triplicate with an uncertainty of <2 %: it excluded the outliers and recorded the average readings. Our replicates suggested that the coefficient of variation was below 2 % in the selected UV–visible spectrum. Given the instrument-specific biases, manufacturer's correction factors allowed us to convert the *S/R* readings into corrected Sc/Rc. We corrected EEM inner-filter effect using non-linear function fits based on absorbance scans (Murphy et al., 2010; Xu et al., 2016). Absorbance Unit (A.U.) was normalized to Raman Unit (R.U.) using Raman peak area of ultrapure water. Water Raman and Rayleigh scatterings were deducted with regional cut and interpolation (Bahram et al., 2006).

2.6. Statistical analyses

Three distinct datasets i.e., (1) land use and landscape metrics, (2) DIC species, and (3) DOC concentrations and optical properties were performed in statistical analyses. We tested data normality and homogeneity of variance with Kolmogorov-Smirnov and Levene's test, respectively. Data were log-transformed when statistical necessary for normality assumptions. We compared statistical differences between distinct seasons and rivers using Mann–Whitney *U* test and Analysis of variance. PARAFAC was modeled using MATLAB in DOMFluor toolbox 1.71 (Stedmon and Bro, 2008).

Random forest model was used to identify relative importance of land use and landscape metrics on dissolved C, further deciphering anthropogenic influences on riverine DIC and DOC biogeochemistry. The random forest was developed from Bootstrap Aggregation (Hu et al., 2022), which is available in high-dimensional estimate of variablesing anthropogenic influThe minimum leaf node size and number of trees were set to be 2 and 500, respectively. The increased errors driven by permuting variables were defined as weights of relative importance. We ran the model multiple times and determine weights using the average values, which might provide a comprehensive assessment regarding primary human contributions to individual dissolved C parameters. In this study, random forest model was performed using MATLAB algorithm, and the visualization of logistic regression was shown in Fig. S1. Statistical analyses were performed using SPSS statistical package (19.0). All the figures were prepared using OriginPro and MATLAB.

3. Results

3.1. Land use and landscape metrics

Our data show that land use types were significantly distinct between the catchments (Table 1). The river Furong had a highest land use proportion of forest (55.3 % ± 18.0 %, mean ± s.d.), and followed by farmland (34.4 % ± 12.7 %). In contrast, farmland was widespread in the river Pengxi, with a dominant proportion of 52.9 % ± 15.7 %, and forest occupied averagely 30.3 % ± 16.2 %. These proportions varied across sampling locations in a broad range, exhibiting a gradual invasion of agricultural to natural land use. Urbanization as another potential man-made perturbation, was notably greater in the Pengxi than Furong with the proportions of 1.81 % ± 3.08 % and 0.32 % ± 0.73 %, respectively ($p < 0.05$, Mann–Whitney *U* test). Grassland proportions spanned 4 orders of magnitude, ranging from 0.01 % to ~36 %. Waters occupied a higher proportion in the Pengxi (2.78 % ± 3.36 %) as compared to the Furong (1.34 % ± 1.02 %), resulting in surface water areas of 59.5 and 46.5 km^2, respectively ($p < 0.05$). It is worth noting that we excluded non-river surface waters e.g., lakes, reservoirs and ponds. The proportions of unused land were mostly low (<1 %) across sampling locations.

Table 1
Comparison of land use proportions and landscape metrics in the karst rivers.

	n	Min	Max	Median	Mean	Std. Dev
Furong River						
Farmland (%)	32	14.6	68.6	33.5	34.4	12.7
Forest (%)	32	11.4	85.0	54.9	55.3	18.0
Grass (%)	32	0.01	36.0	4.47	8.68	10.1
Water (%)	32	0.22	4.35	0.94	1.34	1.02
Urban (%)	32	0.01	4.01	0.04	0.32	0.73
Unused (%)	32	0.01	0.08	0.01	0.014	0.017
TA (km^2)	32	2477	69,657	10,332	14,600	15,706
NP	32	32	711	137	178	153
PD (N/ha)	32	0.56	2.58	1.41	1.47	0.46
LPI (%)	32	14.45	84.5	32.4	35.0	15.8
ED (m/ha)	32	16.7	50.6	38.2	37.0	7.00
AI (%)	32	92.5	97.4	94.3	94.5	1.01
SHDI	32	0.44	1.2	0.87	0.87	0.19
Pengxi River						
Farmland (%)	36	24.4	85.0	51.3	52.9	15.7
Forest (%)	36	3.00	63.0	28.6	30.3	16.2
Grass (%)	36	0.01	36.8	9.21	11.4	9.57
Water (%)	36	0.27	13.0	1.18	2.78	3.36
Urban (%)	36	0.01	15.8	0.59	1.81	3.08
Unused (%)	36	0.01	18.6	0.01	0.89	3.51
TA (km^2)	36	933	35,979	10,835	13,019	9560
NP	36	26	307	137	138	73
PD (N/ha)	36	0.57	4.07	1.10	1.43	0.92
LPI (%)	36	12.9	75.0	39.8	40.6	17.2
ED (m/ha)	36	17.7	80.9	45.5	46.2	16.9
AI (%)	36	88.1	97.3	93.2	93.1	2.50
SHDI	36	0.59	1.40	1.00	1.00	0.20

Landscape metrics ED and SHDI were higher in the Pengxi (46.2 ± 16.9 m/ha; 1.00 ± 0.20) than Furong (37.0 ± 7.00 m/ha; 0.87 ± 0.19), whereas AI presented as Furong (94.5 % ± 1.01 %) > Pengxi (93.1 % ± 2.50 %) ($p < 0.05$). This suggested more diverse land use types and highly fragmented landscape in the Pengxi, in tune with its intensive human activities. Other landscape metrics, however, showed no significant differences between the Furong and Pengxi ($p > 0.05$). We found that TA, NP, PD and LPI values were generally in wide ranges i.e., > threefold variation across sampling locations, with median values of 10,332 km^2, 137, 1.41 N/ha and 32.4 % in the Furong, and 10,835 km^2, 137, 1.10 N/ha and 39.8 % in the Pengxi.

3.2. River DIC chemistry and CO_2 emission

Aqueous DIC concentrations were higher in the dry season (Furong: 2674.5 ± 424.0 μmol/L; Pengxi: 2354.1 ± 448.6 μmol/L) in comparison to rainy season (Furong: 1466.0 ± 285.7 μmol/L; Pengxi: 1217.3 ± 253.7 μmol/L) ($p < 0.001$, Fig. 2). Meanwhile, we found that a spatial difference of DIC presented as Furong > Pengxi ($p < 0.05$). The bulk of river DIC was derived from HCO_3^-, comprising 61–96 % with an average of 92 % ± 6 % of the overall concentrations. Therefore, spatiotemporal HCO_3^- were highly consistent with DIC dynamics. Aqueous CO_3^{2-} varied by 3 orders of magnitude ranging within 0.39–368.7 μmol/L. Observed dissolved CO_2 concentrations exhibited notably temporal variations in the river Furong (dry season 170.5 ± 204.0 > rainy season 31.5 ± 20.1 μmol/L, $p < 0.001$) and Pengxi (dry season 131.2 ± 196.3 > rainy season 60.4 ± 97.7 μmol/L, $p = 0.05$), and yet had no spatial shifts between the rivers ($p > 0.05$). This may indicate that carbonate-dominated rivers share common CO_2 drivers despite spatial isolation. Specifically, DIC species tended to fluctuate in adjacent areas of river damming along the main stem, suggesting a noticeable disturbance to the river continuum (Fig. S2).

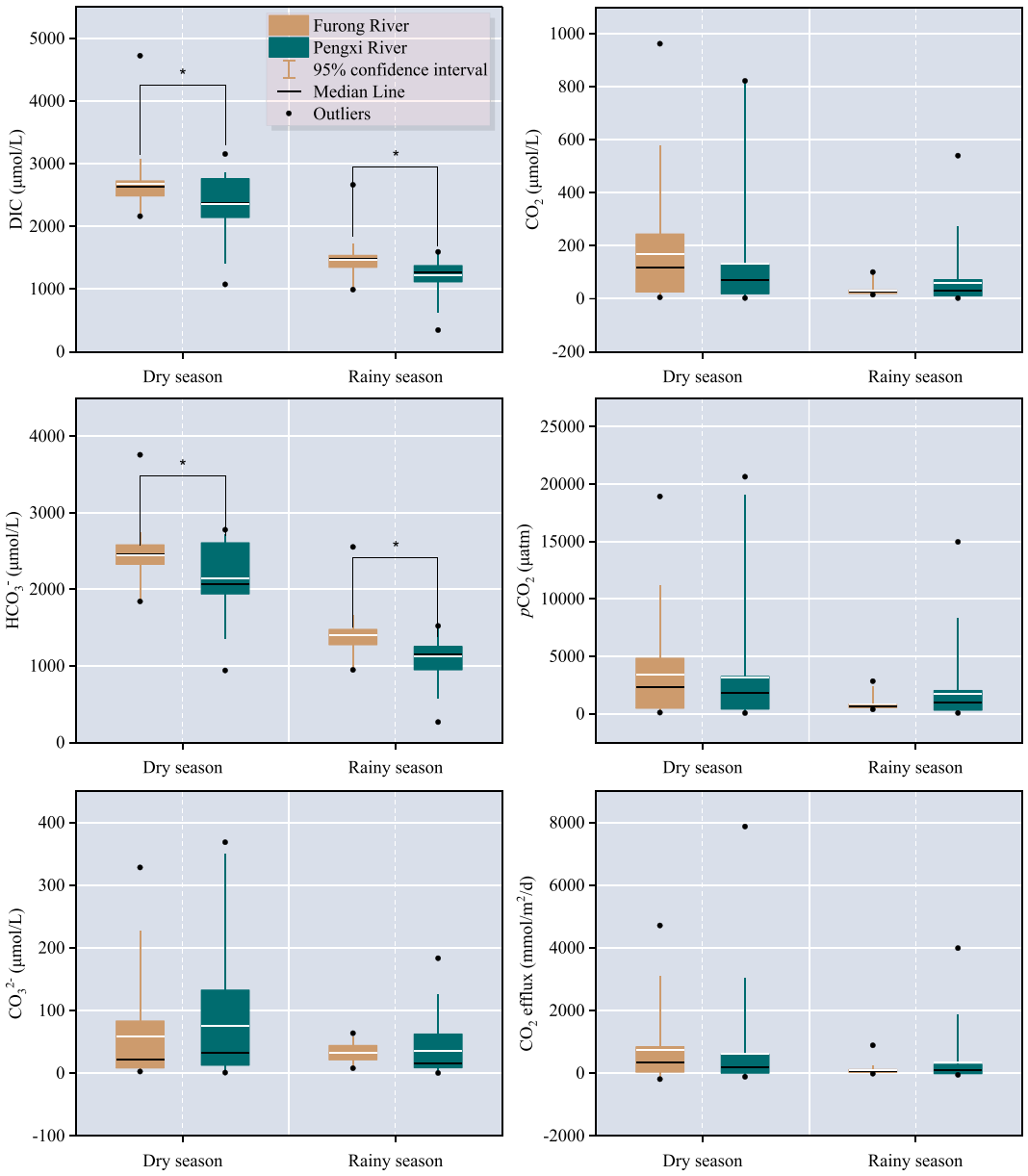

Fig. 2. Spatial and temporal variability of DIC chemistry and water-air CO_2 exchange in the karst rivers (The boxes with whiskers illustrate 25th–75th with 5th–95th percentiles, and the scatters present the outliers. The white and black lines show mean and median values, respectively. The mark * refers to significant difference at $p < 0.05$ level).

River CO_2 exchange was highly variable, and spanned a wide spectrum of pCO_2 and CO_2 efflux. For example, instantaneous pCO_2 levels ranged from 66.0 to 20,642.4 μatm and averaged at 2319.8 ± 3580.1 μatm (Fig. S3). Our data indicate that the median pCO_2 was 0.38 and 0.24–0.74 times the large-scale rivers from global (Raymond et al., 2013) and China's reports (Ran et al., 2021), respectively. Regarding spatiotemporal scales of the datasets, we found the higher pCO_2 in the dry season (Furong: 3395.8 ± 4006.5 μatm; Pengxi: 3183.4 ± 4753.1 μatm) than rainy season (Furong: 842.9 ± 550.3 μatm; Pengxi: 1742.7 ± 2762.9 μatm) ($p < 0.05$). The modeled k varied from 2.9 to 25.8 m/d with a mean of 7.67 ± 4.89 m/d across sampling locations (Fig. S4), which was slightly higher than those for global rivers and streams i.e., 5.7 m/d (Raymond et al., 2013). By merging the paired pCO_2 and k values from our datasets, we calculated areal CO_2 efflux ranging between −58.6 and 2044.5 mmol/m^2/d (95 % confidence intervals) with an average of 452.1 ± 997.5 mmol/m^2/d (Fig. 3). Similarly, it temporally showed dry season > rainy season in the river Furong (743.2 ± 1111.8 > 101.7 ± 158.5 mmol/m^2/d) and Pengxi (607.5 ± 1378.0 > 333.8 ± 737.9 mmol/m^2/d). Particularly, river damming induced a sudden increase of pCO_2 and CO_2 efflux, highly mediating water-air CO_2 outgassing (Fig. S2). In this context, we estimated total CO_2 efflux to be 0.32 ± 0.064 and 0.45 ± 0.11 Tg CO_2/y in the river Furong and Pengxi, respectively.

3.3. River DOC concentrations and optical properties

River DOC concentrations ranged from 90.3 to 656.9 μmol/L across samples, which significantly varied over time (dry season > rainy season) and space (Pengxi > Furong) ($p < 0.05$, Table 2). Aqueous a_{440}, a proxy for lignin-DOC (Derrien et al., 2019), was higher in the Pengxi (5.13 ± 1.60 m^{-1}) when compared to Furong (4.59 ± 1.89 m^{-1}) ($p < 0.05$). The increased $S_{275-295}$ links to photobleaching and decreased DOC molecular weight (Helms et al., 2008), which exhibited variable seasonality in the Furong (Dry season > rainy season) and Pengxi (dry

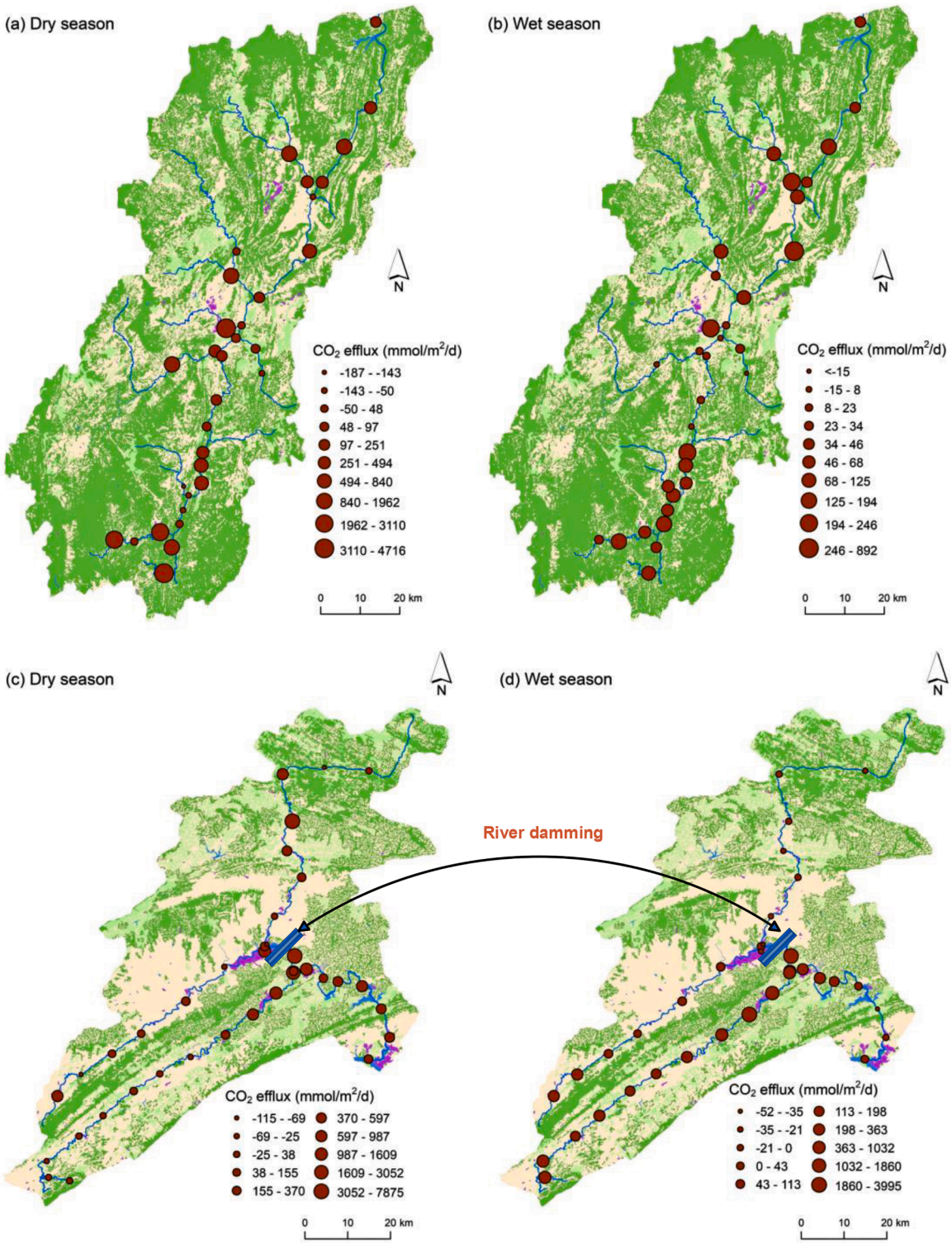

Fig. 3. Spatial distribution of river CO_2 efflux along the karst rivers (a. areal CO_2 efflux in the Furong, dry season; b. areal CO_2 efflux in the Furong, rainy season; c. areal CO_2 efflux in the Pengxi, dry season; d. areal CO_2 efflux in the Pengxi, rainy season).

season < rainy season). Our URI data presented high abundance of unsaturated compounds (Ni and Li, 2022), varying from 3.53 to 408.0 with a mean of 40.1 ± 70.1. We thus suggest that DOC was highly degradable and bioavailable in the dry season, Furong River (median URI = 91.8).

By modeling and comparing PARAFAC components between our datasets and the recorded studies in OpenFluor, we were able to identify primary DOC composition in the karst rivers (Fig. S5). We found that UV humic-like (C1, Ex = 245 nm, Em = 408 nm), terrestrial humic-like (C2, Ex = 260 nm, Em = 458 nm) and tryptophan-like DOC (C2, Ex = 230/275 nm, Em = 332 nm) were collective DOC compositions (Fig. S5). Specifically, C1 was previously reported in biology- and human-impacted rivers (Batista-Andrade et al., 2023; Ni and Li, 2023), while C2 closely matched DOC component in terrestrial and marine and ecosystems (Lei et al., 2021; Sharma et al., 2017). Most studies suggested that C3 was sourced from biological metabolism, which was also

Table 2
Summary of DOC concentrations and optical parameters in the karst rivers.

	n	Min	Max	Median	Mean	Std. Dev
Furong river, dry season						
DOC (μmol/L)	33	188.9	430.04	261.2	269.9	51.9
a_{440} (m^{-1})	33	3.89	5.78	4.61	4.65	0.56
$S_{275-295}$ (nm^{-1})	32	0.0014	0.048	0.0088	0.013	0.011
URI	28	35.9	408.0	91.8	133.7	109.0
Furong river, rainy season						
DOC (μmol/L)	32	90.3	324.3	236.0	217.6	68.6
a_{440} (m^{-1})	32	0.48	9.37	4.28	4.53	2.65
$S_{275-295}$ (nm^{-1})	32	0.002	0.011	0.009	0.0079	0.0026
URI	32	15.5	36.6	25.4	25.0	5.30
Pengxi river, dry season						
DOC (μmol/L)	37	216.1	656.9	394.9	369.5	82.7
a_{440} (m^{-1})	37	4.08	7.08	5.16	5.32	0.82
$S_{275-295}$ (nm^{-1})	37	0.0002	0.011	0.007	0.0069	0.0033
URI	37	4.31	93.6	12.5	16.7	18.8
Pengxi river, rainy season						
DOC (μmol/L)	35	118.0	460.7	214.3	240.3	84.7
a_{440} (m^{-1})	35	0.55	8.64	4.61	4.93	2.13
$S_{275-295}$ (nm^{-1})	35	0.009	0.016	0.012	0.012	0.0015
URI	35	3.53	12.6	6.96	7.47	2.63

interpreted as protein-like DOC (Fouché et al., 2020; Graeber et al., 2021). Given significant signals of biologically derived DOC (as also indicated by F_{max}, Fig. S6) across samples, we underline that DOC was governed by biotic drivers in karst river.

Taking DOC analysis a step further, the full-region fluorophores were compiled and apportioned, *via* fluorescence regional integration (Fig. 4). Here we calculated proportions of distinct DOC compositions by identifying their corresponding EEM areas. Consistent with PARAFAC models, humic-like DOC (region V) was assumed to be a fundamental contributor occupying 30 %–63 % of DOC fluorophores across samples. Biogenic DOC i.e., tyrosine- (region I), tryptophan- (region II) and microbial byproduct-like compositions (region IV) collectively contributed 16–59 % and were more abundant in the river Furong than Pengxi ($p < 0.001$). By contrast, terrigenous fulvic acid-like DOC ranged within 11–26 %, which was temporally higher in the dry season than rainy season ($p < 0.001$, Fig. S7). River β:α and HIX varied within the range of 0.7–1.0 and 0.1–0.9, respectively (Fig. 5). The highest β:α was observed in the dry season (Furong River), whereas HIX was spatially higher in the river Pengxi. We found that river damming accelerate biological metabolism of DOC, as characterized by the variations in paired biogenic DOC-β:α and humic DOC–HIX (Fig. S8).

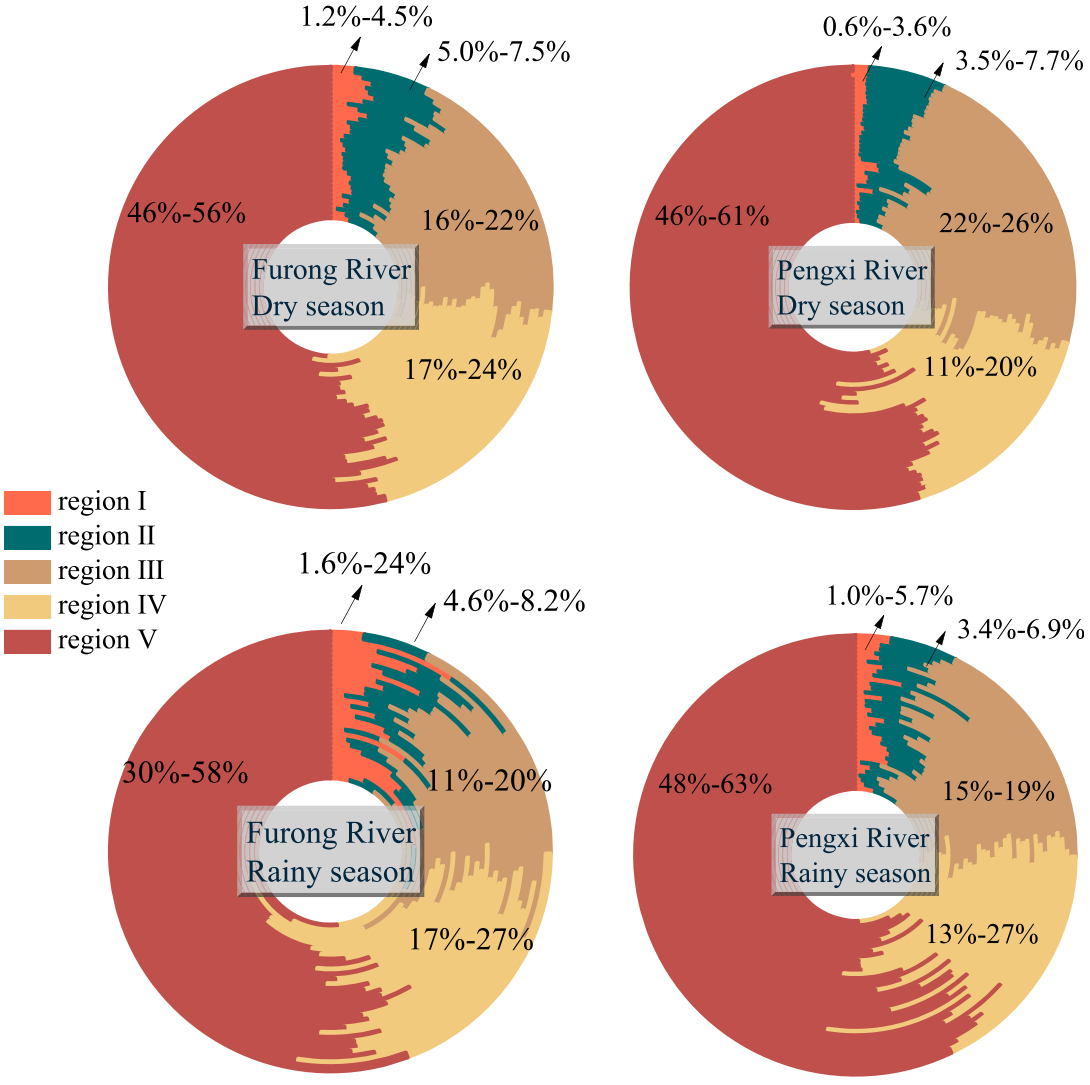

Fig. 4. Proportions of tyrosine- (region I), tryptophan- (region II), fulvic acid- (region III), soluble microbial byproduct-like (region IV) and humic-like DOC (region V) in the karst rivers.

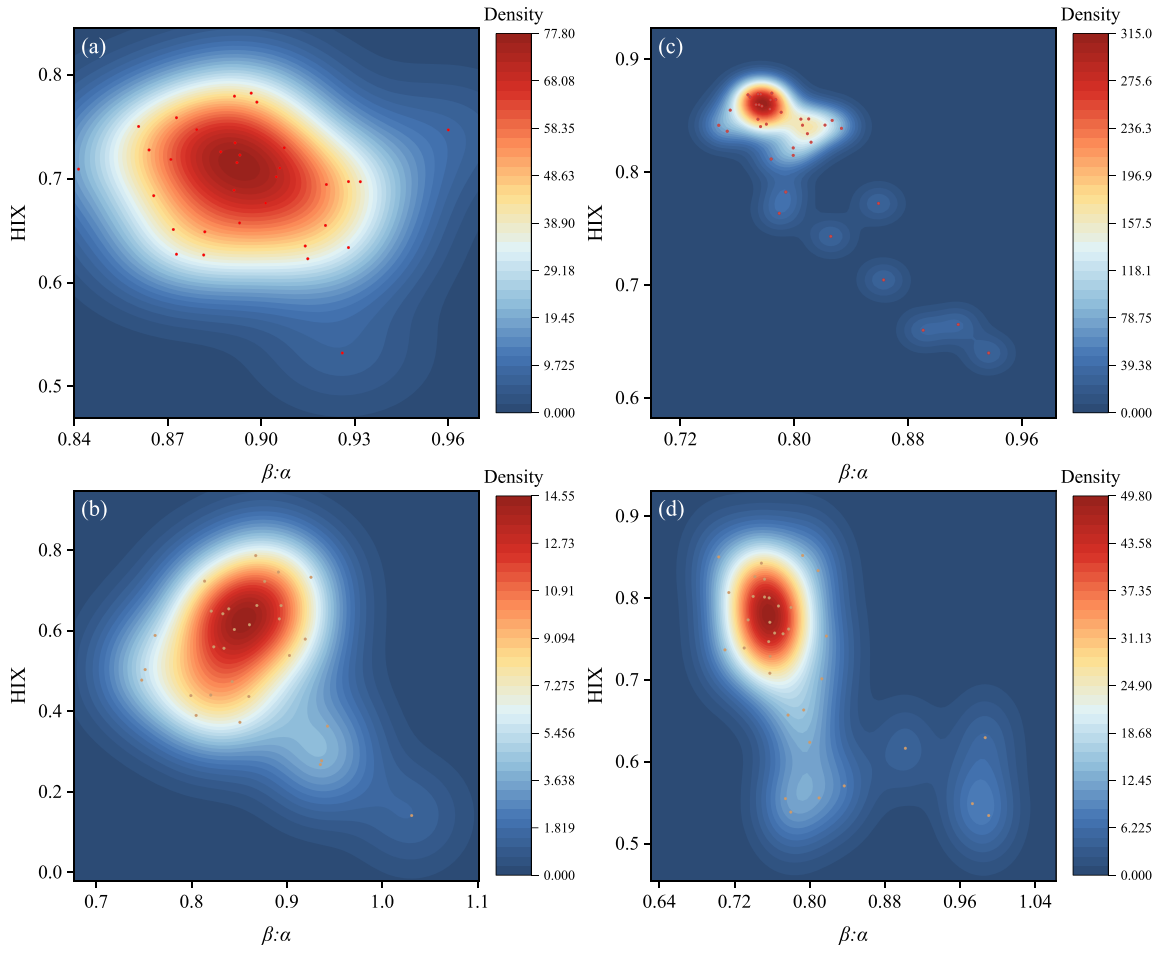

Fig. 5. Distribution density of river freshness index (β:α) and humification index (HIX) in the karst rivers (letters a, b, c and d are similar to Fig. 3).

4. Discussion

4.1. Human-induced variations in DIC biogeochemistry

River DIC turnover linking water chemistry with biology have specific pathways in karst and semi-karst regions. For instance, the known "biological C pump" drives aquatic uptake of DIC for primary production (Sun et al., 2021), resulting in large consumption of HCO_3^- and dissolved CO_2 (Fig. 2). This was supported by the co-dynamics of dissolved oxygen (Fig. S9), expressed as $CaCO_3 + CO_2 + H_2O \rightarrow Ca^{2+} + 2HCO_3^- \rightarrow CaCO_3 + x\,(CO_2 + H_2O) + (1-x)\,(CH_2O + O_2)$. It was especially the case for the rainy season (summer, Fig. 2), intense sunlight and rainfall accelerate photosynthesis and carbonate dissolution, respectively (de Montety et al., 2011; Maisonneuve et al., 2022). Thus, river CO_2 emission was apparently modulated by this pathway, consistently showing the areal CO_2 efflux of dry season > rainy season (Fig. 2). The dilution effect (Chaplot and Mutema, 2021) may not be applicable to explain temporal shifts of DIC species in the study river Pengxi, due to the specific water impounding (water level: dry season > rainy season). The karst rivers contributed significantly to CO_2 outgassing in the bulk of drainage networks (Fig. 3). Terrestrially derived CO_2 inputs and in-stream respiration might simply uncover the supersaturated CO_2, given the region-specific soil erosion and biological metabolism (Borges et al., 2015; Lapierre et al., 2013). Those CO_2 drivers are likely equivalent to the studied rivers, causing the comparable pCO_2 and CO_2 efflux despite their spatial isolation (Fig. 3 and S3).

The damming of rivers represents an important anthropogenic disturbance along the river continuum, which alters aquatic biology by shifting water temperature and retention (Regnier et al., 2013). Consequently, we found that DIC species had sudden changes in adjacent areas of river damming (Fig. S2). The activated biological metabolism involves both photosynthesis and respiration (Battin et al., 2023), inducing distinct pathways for DIC turnover between the species. For example, water impounding enhanced photosynthetic DIC uptake (Wang et al., 2022), as reflected by the decline of HCO_3^- (Fig. S2). In contrast, the locations adjacent to the dam sharply became hotspots for CO_2 emissions (Fig. S2). This was in tune with the prevailing view (Maavara et al., 2017; Ran et al., 2017), suggesting that river dams impelled organic C mineralization. For given land use and landscape metrics (Table 1), relative importance of anthropogenic stresses on river DIC shifts was assessed by machine learning, random forest model. We show that agricultural land use largely modulated DIC in the karst rivers, as indicated by direct farmland to HCO_3^- (Fig. 6a) and agricultural patch-derived LPI to DIC species (Fig. 6c). Indeed, agriculture increased mineral and alkalinity inputs (Chen et al., 2021b; Ran et al., 2015), altering DIC species and the corresponding pH-driven dynamics ($CO_2 + H_2O \leftrightarrow H_2CO_3 \leftrightarrow H^+ + HCO_3^- \leftrightarrow 2H^+ + CO_3^{2-}$). The PD, ED, AI and SHDI linked to pCO_2 (Fig. 6), indicating that diverse and fragmented patches potentially contributed to river CO_2 emissions. Landscape area plays a fundamental role in modulating dissolved C dynamics, which is highly constrained by artificial land use e.g., land development and deforestation. Thus, we specifically found that TA was associated with DIC concentration and HCO_3^- in the high human-stress river (Fig. 6c and d).

4.2. Human-induced variations in DOC biogeochemistry

Our data indicate that aquatic DOC was highly active and variable in the karst rivers. Anthropogenic activities enhanced land-water

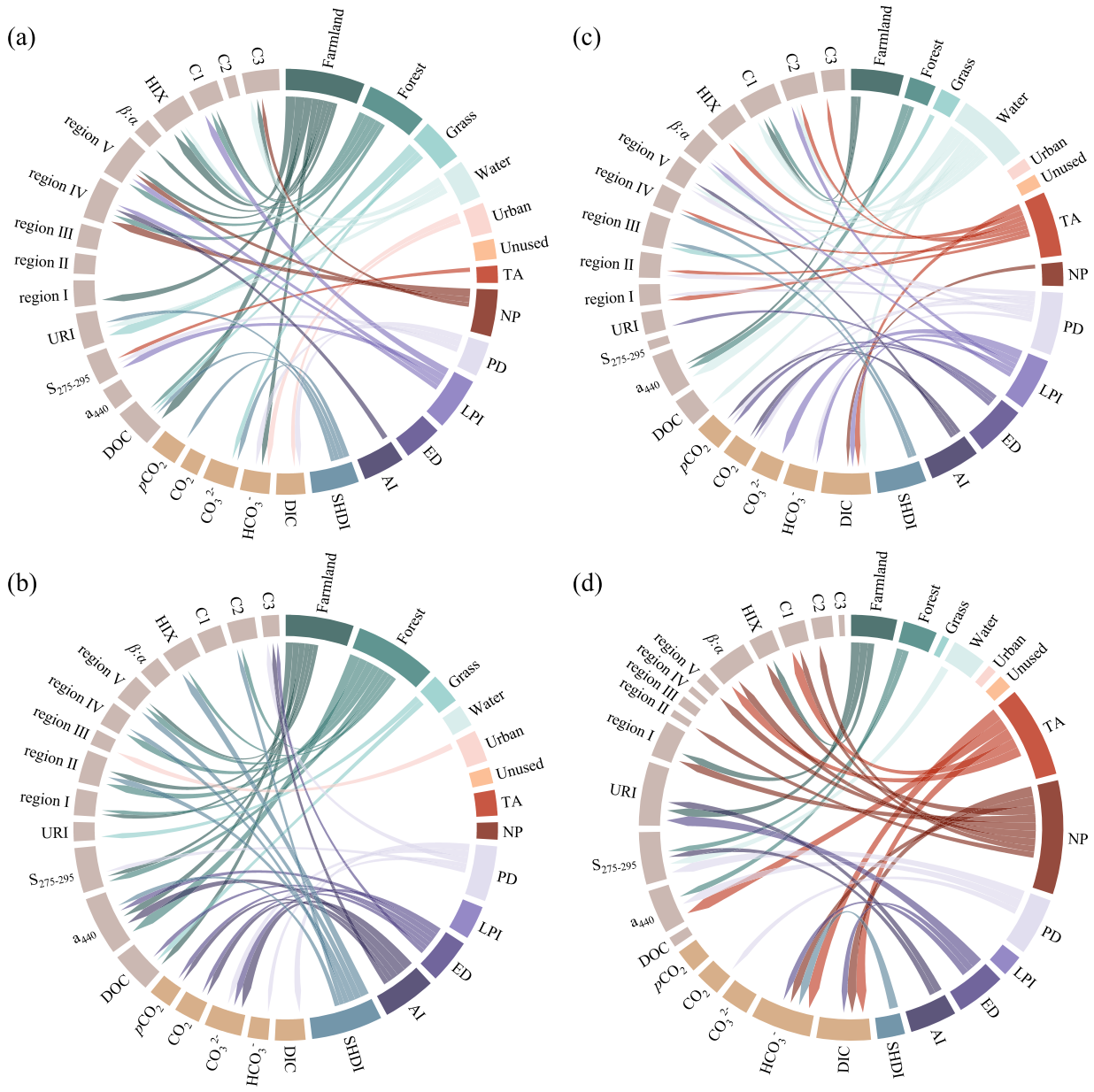

Fig. 6. Machine learning-based relative importance of anthropogenic stresses to river dissolved carbon in the karst rivers (letters a, b, c and d are similar to Fig. 3. The flows represent the top 20 % weights of relative importance from land use and landscape metrics to dissolved C chemistry, as supplied by random forest model).

connectivity (Zhou et al., 2021), causing accumulated terrigenous lignin and DOC concentrations in the high human-stress river Pengxi (Table 2). We found biologically derived i.e., UV humic- and tryptophan-like compositions as universal DOC in the rivers (Fig. S5). This was confirmed by 16–59 % proportion of biogenic DOC (Fig. 4) and high β:α values (Fig. 5). A recent study suggested that UV humic-like component represented as a transition state during DOC biodegradation (Ni and Li, 2023). We thus speculated that in tune with the emerging view (Hu et al., 2023), river DOC undergone a continuous decay regarding incomplete degradation and even biological mineralization. This process was particularly pronounced in the dry season, leading to relative accumulation of terrigenous fulvic acid-like DOC (Fig. S7), a recalcitrant compound in natural waters.

This study provides empirical evidence that river DOC varied dramatically after flowing the river dam. For instance, river damming reinforced DOC bioavailability and freshness, and yet relatively reduced abundance of humic-like DOC and thus humification (Fig. S8). Long-term retention was assumed to exhaust labile DOC and result in extreme lack of organic C substrate (Catalán et al., 2016). From this perspective, running waters might accommodate the sudden interruption and retention by utilizing aquatic DOC deeply rather than having "fast food". These observations indicated that human-induced water retention highly stimulated DOC biodegradation (Kida et al., 2019; Zheng et al., 2020). Our results show that farmland and forest were primary contributors for macromolecular humic-like DOC (region V and HIX) and terrigenous lignin (a_{440}) in the rivers (Fig. 6). Particularly, agriculture had significant weights on mediating biogenic fluorescence signatures (region I, II and β:α), as observed in other streams despite the distinct DOC characterization i.e., ultrahigh-resolution mass spectrometry (Spencer et al., 2019). This was in good agreement with previous findings (Clark et al., 2022; Humbert et al., 2020; Wilson and Xenopoulos, 2009), suggesting agriculture increased DOC structural complexity and biodegradability. We observed that DOC chemistry was less susceptible to farmland and forest in the Pengxi (Fig. 6c and d),

probably because the mixed landscapes masked the flows driven by individual land uses in the high human-stress river. Particularly, AI served as a universal indicator associated with diverse DOC compositions across space and time (Fig. 6). This reflects that the growing fragmentation of land use contribute to riverine DOC diversity.

4.3. Dissolved C turnover driven by anthropogenic disturbances

Inner linkages of DIC with DOC can reveal dissolved C turnover between inorganic and organic phases in aquatic systems (Ni and Li, 2022). Here, we observed their co-dynamics driven by biological production and degradation (Fig. 7). Our results upscale that "biological C pump" not only stimulated primary production e.g., carbohydrates, but also triggered overall organic C turnover. Aquatic DIC species linked to biogenic (protein- and microbial byproduct-like) DOC components, unsaturated compounds (URI) and freshness (β:α) (Fig. 7), indicating primary production accelerated biological metabolism (Tortell et al., 2014; Zhong et al., 2021). The strong associations of CO_2 (pCO_2) with lignin (Fig. 7b) and DOC molecular weight (Fig. 7c) further confirm terrestrial inputs and DOC biodegradation acting as primary CO_2 sources in the karst rivers. However, these processes in turn promoted recalcitrant DOC accumulation, as reflected by negative relationships between DIC/HCO_3^- and humic-like DOC (Fig. 7c and d). Given the diverse relationships among dissolved C chemistry, we provide a causal description and analysis in Supplementary Information S2.

Artificial dams extended hydraulic retention time, accelerating both photosynthetic DIC uptake (Fig. S2) and biological DOC degradation (Fig. S8). For the karst rivers, damming caused more CO_2 generation than consumption, as supported by potential CO_2 emissions (Fig. S2). In this study, we identified anthropogenic disturbances on dissolved C turnover as the flows from land use and landscape metrics (Fig. 6) to the linked DIC and DOC (Fig. 7). We found farmland modulated the co-trajectory of HCO_3^- consumption and tyrosine-like DOC generation in the low human-stress river (Figs. 6a and 7a). In comparison, agricultural patch-derived LPI apparently stimulated synergistic DOC biodegradation (C2 and β:α) with DIC (DIC and HCO_3^-) increase in the high human-stress river (Figs. 6c and 7c). These results evidenced that agriculture unexpectedly led to hybrid functions on dissolved C interactions. Human-induced land use changes (TA) drove biologically derived DIC-DOC transformation in the dry season (Fig. 6c), and yet affected terrestrial DIC-DOC inputs in the rainy season (Fig. 6d). Therefore, fluvial DIC-DOC evolution was seasonally constrained by anthropogenic disturbances. The relatively aggregated land-use patches (AI) enhanced land-water connectivity, which intensified terrestrial pathway of CO_2

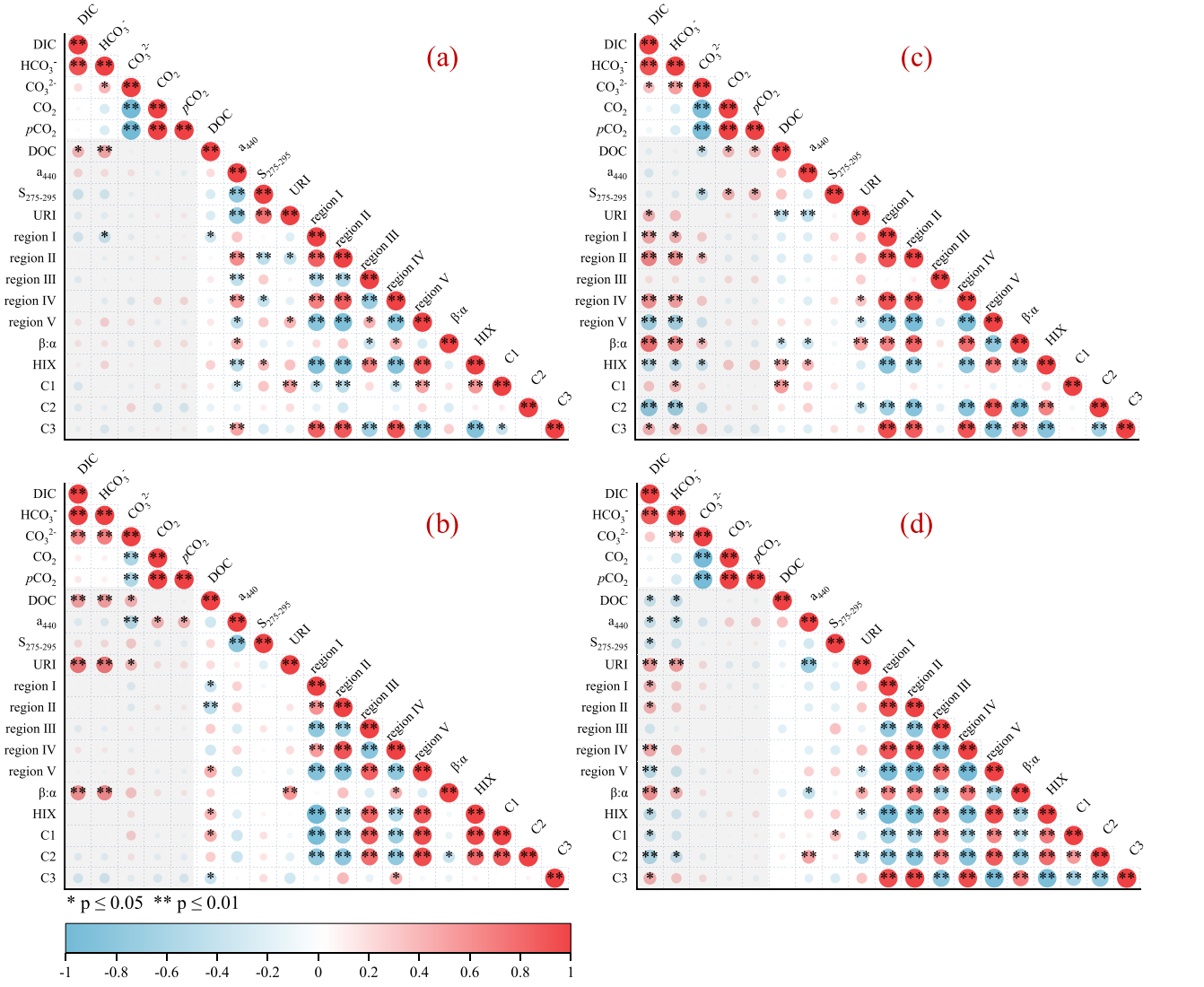

Fig. 7. Spearman's correlations of DIC species with DOC chemistry in the karst rivers (letters a, b, c and d are similar to Fig. 3. The red and blue circles with * $p <$ 0.05 or ** $p <$ 0.01 indicate significant positive and negative correlations between the corresponding parameters, respectively).

and lignin inputs in the low human-stress river (rainy season, Figs. 6a and 7a). For more detailed information on modeling the relative importance of anthropogenic stresses to dissolved C please see Fig. S10.

4.4. Implications for river C cycling

The C allocation in karst rivers driven by DIC and DOC turnover, along with the specific conversion pathways involved, is highly susceptible to anthropogenic disturbances. In this study, we show that river dissolved C shifts followed the associated trajectories of biogeochemistry, with important implications for aquatic C cycles. For instance, karst waters constitute a substantial DIC pool supply for coupled carbonate dissolution with photosynthesis, leading to large CO_2 consumption for primary production (Liu et al., 2015). Rainfall synergistically effects on CO_2 sink and results in seasonal patterns of river CO_2 reserves (Liu et al., 2010). The photosynthetic products e.g., carbohydrates are bio-labile and apparently stimulate biological metabolism, causing co-dynamics of overall DOC compositions (Fig. 7). That is, "biological C pump" unexpectedly drove rapid utilization of bioavailable and semi-labile DOC. With large biogenic signals, partial DOC undergoes incomplete degradation, and the remaining is mineralized into CO_2. The produced CO_2 will be in turn consumed by the combined action of carbonate dissolution with photosynthesis, establishing a complete cycle of dissolved C.

From this perspective, we introduce a process-based conceptual model, the rapid cycle of active C in karst waters (Fig. 8). It is supposed to have a part of dissolved C rapidly cycling in karst and semi-karst aquatic ecosystems: 1) carbonate dissolution sequesters CO_2 as HCO_3^- form ($CaCO_3 + CO_2 + H_2O \rightarrow Ca^{2+} + 2HCO_3^-$); 2) photosynthetic uptake of HCO_3^- produces bio-labile CH_2O ($Ca^{2+} + 2HCO_3^- \rightarrow CaCO_3 + CH_2O + O_2$); 3) aquatic respiration of DOC preferentially utilizes bioavailable CH_2O ($CH_2O + O_2 \rightarrow CO_2 + H_2O + ATP$); 4) the bulk of produced CO_2 will be feedback to carbonate dissolution. The sequent processes (1) and (2) were well-understood by previous studies (Marcé et al., 2015; Song et al., 2022). Nevertheless, we underline that the processes (2) and (3) serve as key trajectories linking DIC and DOC turnover, and give a knowledge response to why karst rivers consume such a large CO_2 but still represent as CO_2 emitters — the rapid cycle of active C not only makes a substantial promotion for labile DOC mineralization, but also triggers overall DOC metabolism in karst rivers. Thus, the net CO_2 sink arising from "biological C pump" is partially counteracted by the activated biology.

Anthropogenic activities e.g., river damming and agricultural practice, nevertheless, accelerate the rapid cycle of active C, largely changing karst river dissolved C turnover. Consistent with our hypothesis, human activities altered dissolved C by disturbing the associated trajectories of DIC and DOC biogeochemistry. Given full pathways of man-made shifts in DIC and DOC turnover are still obscure (Bernot et al., 2010; Maavara et al., 2017), our study provides a novel understanding of the mechanistic underpinning regarding C cycling in karst waters. Human disturbances actively mobilise mutual transformations of the active C between inorganic and organic forms, particularly for

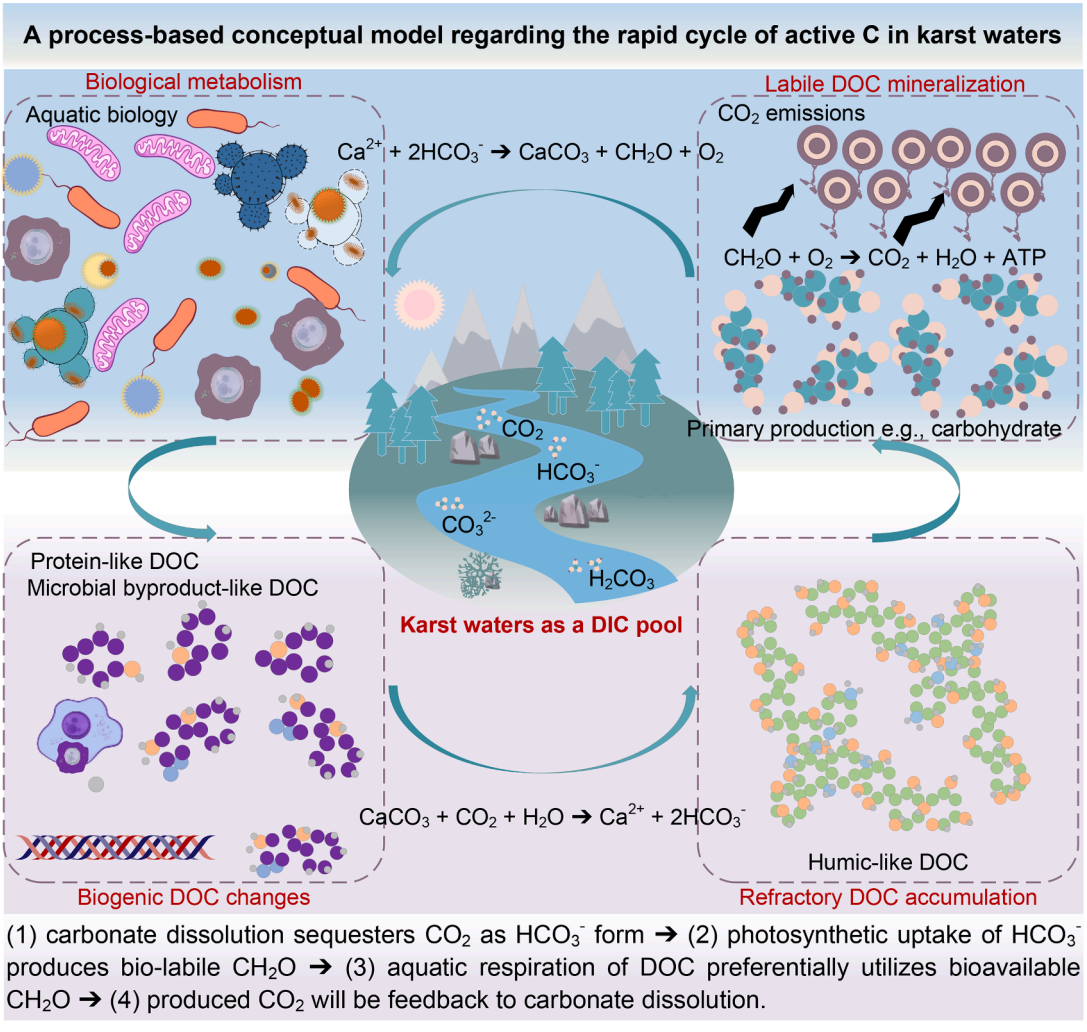

Fig. 8. A process-based conceptual model regarding the rapid cycle of active C in karst waters.

mineralizing DOC into CO_2. Therefore, this study suggests that reducing anthropogenic stimulation on natural waters may decompress dissolved C turnover, and further sequester aquatic CO_2 in the context of global C neutrality.

5. Conclusion

Karst river dissolved C turnover was driven by the specific biogeochemical pathways, which showed the substantial shifts in response to human-induced disturbances. Here, we demonstrated that river damming and land use stimulated biological metabolism, highly altering DIC and DOC characteristics in the karst waters. Anthropogenic activities exhibited synchronous accelerations to aquatic photosynthesis and respiration, ultimately causing more river CO_2 production than fixation. River damming reinforced DOC bioavailability, while agriculture increased DOC structural complexity. Artificial dams and land uses unexpectedly altered aquatic DIC-DOC transformation. Based on these findings, we proposed a process-based conceptual model, indicating that a part of dissolved C is cycled rapidly in karst and semi-karst aquatic ecosystems. This study suggests that restricting human disturbances on natural waters can decompress dissolved C turnover and sequester CO_2 emissions in the context of global C neutrality.

Declaration of Competing Interest

All authors agree this submission and the authors declare that there is no conflict of interests regarding the publication of this article

Data availability

Data will be made available on request.

Acknowledgments

This study was financially supported by the Strategic Priority Research Program of the Chinese Academy of Sciences (XDB40020200), National Natural Science Foundation of China (NSFC grant no. 42107091 and 42273021), Science and Technology Research Project of Chongqing Municipal Education Commission (KJZD-M202200502, KJQN202200517), Natural Science Foundation of Chongqing, China (CSTB2022NSCQ-LZX0022), Science Foundation of Chongqing Normal University (20XLB022, 21XRC002), and the Second Tibetan Plateau Scientific Expedition and Research Program (Sub-item: 2019QZKK0601-3). Special thanks are given to the editor and anonymous reviewers for their constructive comments and suggestions.

Supplementary materials

Supplementary material associated with this article can be found, in the online version, at doi:10.1016/j.watres.2023.120744.

References

Alin, S.R., Rasera, M.D.F.F.L., Salimon, C.I., Richey, J.E., Holtgrieve, G.W., Krusche, A.V., Snidvongs, A., 2011. Physical controls on carbon dioxide transfer velocity and flux in low-gradient river systems and implications for regional carbon budgets. J. Geophys. Res. Biogeosci. 116 (G1), 248–255.

American Public Health Association (APHA), 1985. Standard Methods for the Examination of Water and Wastewater, 16th ed. American Public Health Association, Washington, DC, p. 1268.

Bahram, M., Bro, R., Stedmon, C., Afkhami, A., 2006. Handling of Rayleigh and Raman scatter for PARAFAC modeling of fluorescence data using interpolation. J. Chemom. 20 (3–4), 99–105.

Batista-Andrade, J.A., Diaz, E., Iglesias Vega, D., Hain, E., Rose, M.R., Blaney, L, 2023. Spatiotemporal analysis of fluorescent dissolved organic matter to identify the impacts of failing sewer infrastructure in urban streams. Water Res. 229, 119521.

Battin, T.J., Lauerwald, R., Bernhardt, E.S., Bertuzzo, E., Gener, L.G., Hall, R.O., Hotchkiss, E.R., Maavara, T., Pavelsky, T.M., Ran, L., Raymond, P., Rosentreter, J.A., Regnier, P., 2023. River ecosystem metabolism and carbon biogeochemistry in a changing world. Nature 613 (7944), 449–459.

Battin, T.J., Luyssaert, S., Kaplan, L.A., Aufdenkampe, A.K., Richter, A., Tranvik, L.J., 2009. The boundless carbon cycle. Nat. Geosci. 2 (9), 598–600.

Bernot, M.J., Sobota, D.J., Hall Jr, R.O., Mulholland, P.J., Dodds, W.K., Webster, J.R., Tank, J.L., Ashkenas, L.R., Cooper, L.W., Dahm, C.N., Gregory, S.V., Grimm, N.B., Hamilton, S.K., Johnson, S.L., McDowell, W.H., Meyer, J.L., Peterson, B., Poole, G.C., Valett, H.M., Arango, C., Beaulieu, J.J., Burgin, A.J., Crenshaw, C., Helton, A.M., Johnson, L., Merriam, J., Niederlehner, B.R., O'Brien, J.M., Potter, J.D., Sheibley, R. W., Thomas, S.M., Wilson, K.Y.M, 2010. Inter-regional comparison of land-use effects on stream metabolism. Freshw. Biol. 55 (9), 1874–1890.

Borges, A.V., Darchambeau, F., Teodoru, C.R., Marwick, T.R., Tamooh, F., Geeraert, N., Omengo, F.O., Guérin, F., Lambert, T., Morana, C., Okuku, E., Bouillon, S., 2015. Globally significant greenhouse-gas emissions from African inland waters. Nat. Geosci. 8, 637–642.

Butman, D.E., Wilson, H.F., Barnes, R.T., Xenopoulos, M.A., Raymond, P.A., 2015. Increased mobilization of aged carbon to rivers by human disturbance. Nat. Geosci. 8 (2), 112–116.

Butscher, C., Huggenberger, P., 2008. Intrinsic vulnerability assessment in karst areas: a numerical modeling approach. Water Resour. Res. 44 (3).

Campeau, A., Bishop, K.H., Billett, M.F., Garnett, M.H., Laudon, H., Leach, J.A., Nilsson, M.B., Öquist, M.G., Wallin, M.B., 2017. Aquatic export of young dissolved and gaseous carbon from a pristine boreal fen: implications for peat carbon stock stability. Glob. Change Biol. 23 (12), 5523–5536.

Catalán, N., Marcé, R., Kothawala, D.N., Tranvik, L.J., 2016. Organic carbon decomposition rates controlled by water retention time across inland waters. Nat. Geosci. 9 (7), 501–504.

Chaplot, V., Mutema, M., 2021. Sources and main controls of dissolved organic and inorganic carbon in river basins: a worldwide meta-analysis. J. Hydrol. (Amst.) 603, 126941.

Chen, S., Zhong, J., Li, C., Liu, J., Wang, W., Xu, S., Li, S.-L., 2021a. Coupled effects of hydrology and temperature on temporal dynamics of dissolved carbon in the Min River. Tibetan Plateau. J. Hydrol. 593, 125641.

Chen, S., Zhong, J., Li, S., Ran, L., Wang, W., Xu, S., Yan, Z., Xu, S., 2021b. Multiple controls on carbon dynamics in mixed karst and non-karst mountainous rivers, Southwest China, revealed by carbon isotopes (δ13C and Δ14C). Sci. Total Environ. 791, 148347.

Clark, K.E., Stallard, R.F., Murphy, S.F., Scholl, M.A., González, G., Plante, A.F., McDowell, W.H., 2022. Extreme rainstorms drive exceptional organic carbon export from forested humid-tropical rivers in Puerto Rico. Nat. Commun. 13 (1), 2058.

Coble, A.A., Wymore, A.S., Potter, J.D., McDowell, W.H., 2022. Land Use Overrides stream order and season in driving dissolved organic matter dynamics throughout the year in a river network. Environ. Sci. Technol. 56 (3), 2009–2020.

Pierrot, D.E., Wallace, D.W.R., Lewis, E., 2006. MS Excel Program Developed for CO_2 System Calculations. ORNL/CDIAC-105a. Carbon Dioxide Information Analysis Center. Oak Ridge National Laboratory, U.S. Department of Energy, Oak Ridge, Tennessee.

de Montety, V., Martin, J.B., Cohen, M.J., Foster, C., Kurz, M.J., 2011. Influence of diel biogeochemical cycles on carbonate equilibrium in a karst river. Chem. Geol. 283 (1–2), 31–43.

Derrien, M., Brogi, S.R., Gonçalves-Araujo, R., 2019. Characterization of aquatic organic matter: assessment, perspectives and research priorities. Water Res. 163, 114908.

Dornblaser, M.M., Striegl, R.G., 2015. Switching predominance of organic versus inorganic carbon exports from an intermediate-size subarctic watershed. Geophys. Res. Lett 42 (2), 386–394.

Drake, T.W., Podgorski, D.C., Dinga, B., Chanton, J.P., Six, J., Spencer, R.G.M., 2020. Land-use controls on carbon biogeochemistry in lowland streams of the Congo Basin. Global. Change Biol. 26 (3), 1374–1389.

Fouché, J., Christiansen, C.T., Lafrenière, M., Grogan, P., Lamoureux, S.F., 2020. Canadian permafrost stores large pools of ammonium and optically distinct dissolved organic matter. Nat. Commun. 11 (1), 4500.

Graeber, D., Tenzin, Y., Stutter, M., Weigelhofer, G., Shatwell, T., von Tümpling, W., Tittel, J., Wachholz, A., Borchardt, D., 2021. Bioavailable DOC: reactive nutrient ratios control heterotrophic nutrient assimilation—An experimental proof of the macronutrient-access hypothesis. Biogeochemistry 155 (1), 1–20.

Grill, G., Lehner, B., Thieme, M., Geenen, B., Tickner, D., Antonelli, F., Babu, S., Borrelli, P., Cheng, L., Crochetiere, H., Ehalt Macedo, H., Filgueiras, R., Goichot, M., Higgins, J., Hogan, Z., Lip, B., McClain, M.E., Meng, J., Mulligan, M., Nilsson, C., Olden, J.D., Opperman, J.J., Petry, P., Reidy Liermann, C., Sáenz, L., Salinas-Rodríguez, S., Schelle, P., Schmitt, R.J.P., Snider, J., Tan, F., Tockner, K., Valdujo, P. H., van Soesbergen, A., Zarfl, C., 2019. Mapping the world's free-flowing rivers. Nature 569 (7755), 215–221.

Hansen, A.M., Kraus, T.E.C., Pellerin, B.A., Fleck, J.A., Downing, B.D., Bergamaschi, B.A., 2016. Optical properties of dissolved organic matter (DOM): effects of biological and photolytic degradation. Limnol. Oceanogr 61 (3), 1015–1032.

Helms, J.R., Stubbins, A., Ritchie, J.D., Minor, E.C., Kieber, D.J., Mopper, K., 2008. Absorption spectral slopes and slope ratios as indicators of molecular weight, source, and photobleaching of chromophoric dissolved organic matter. Limnol. Oceanogr. 53 (3), 955–969.

Horgby, Å., Segatto, P.L., Bertuzzo, E., Lauerwald, R., Lehner, B., Ulseth, A.J., Vennemann, T.W., Battin, T.J., 2019. Unexpected large evasion fluxes of carbon dioxide from turbulent streams draining the world's mountains. Nat Commun 10 (1), 4888.

Hotchkiss, E.R., Hall, R.O., Sponseller, R.A., Butman, D., Klaminder, J., Laudon, H., Rosvall, M., Karlsson, J., 2015. Sources of and processes controlling CO_2 emissions change with the size of streams and rivers. Nat. Geosci. 8 (9), 696–699.

Hotchkiss, E.R., Sadro, S., Hanson, P.C., 2018. Toward a more integrative perspective on carbon metabolism across lentic and lotic inland waters. Limnol. Oceanogr. Lett. 3 (3), 57–63.
Hu, A., Choi, M., Tanentzap, A.J., Liu, J., Jang, K.-S., Lennon, J.T., Liu, Y., Soininen, J., Lu, X., Zhang, Y., Shen, J., Wang, J., 2022. Ecological networks of dissolved organic matter and microorganisms under global change. Nat. Commun. 13 (1), 3600.
Hu, J., Kang, L., Li, Z., Feng, X., Liang, C., Wu, Z., Zhou, W., Liu, X., Yang, Y., Chen, L., 2023. Photo-produced aromatic compounds stimulate microbial degradation of dissolved organic carbon in thermokarst lakes. Nat. Commun. 14 (1), 3681.
Humbert, G., Parr, T.B., Jeanneau, L., Dupas, R., Jaffrezic, A., 2020. Agricultural practices and hydrologic conditions shape the temporal pattern of soil and stream water dissolved organic matter. Ecosystems 23 (7), 1325–1343.
Kida, M., Kojima, T., Tanabe, Y., Hayashi, K., Kudoh, S., Maie, N., Fujitake, N., 2019. Origin, distributions, and environmental significance of ubiquitous humic-like fluorophores in Antarctic lakes and streams. Water Res. 163, 114901.
Lapierre, J.F., Guillemette, F., Berggren, M., del Giorgio, P.A., 2013. Increases in terrestrially derived carbon stimulate organic carbon processing and CO_2 emissions in boreal aquatic ecosystems. Nat. Commun. 4, 2972.
Lei, J., Yang, L., Zhu, Z., 2021. Testing the effects of coastal culture on particulate organic matter using absorption and fluorescence spectroscopy. J. Clean. Prod. 325, 129203.
Li, S., Xu, Y.J., Ni, M., 2021. Changes in sediment, nutrients and major ions in the world largest reservoir: effects of damming and reservoir operation. J. Clean. Prod. 318.
Li, S.Y., Lu, X.X., He, M., Zhou, Y., Li, L., Ziegler, A.D., 2012. Daily CO_2 partial pressure and CO_2 outgassing in the upper Yangtze river basin: a case study of the Longchuan river. China. J. Hydrol. 466, 141–150.
Liu, H., Liu, Z., Macpherson, G.L., Yang, R., Chen, B., Sun, H., 2015. Diurnal hydrochemical variations in a karst spring and two ponds, maolan karst experimental site, China: biological pump effects. J. Hydrol. (Amst) 522, 407–417.
Liu, S., Kuhn, C., Amatulli, G., Aho, K., Butman, D.E., Allen, G.H., Lin, P., Pan, M., Yamazaki, D., Brinkerhoff, C., 2022. The importance of hydrology in routing terrestrial carbon to the atmosphere via global streams and rivers. Proc. Nation. Acad.Sci. 119 (11), e2106322119.
Liu, Z., Dreybrodt, W., Wang, H., 2010. A new direction in effective accounting for the atmospheric CO_2 budget: considering the combined action of carbonate dissolution, the global water cycle and photosynthetic uptake of DIC by aquatic organisms. Earth-Sci. Rev. 99 (3–4), 162–172.
Longworth, B.E., Petsch, S.T., Raymond, P.A., Bauer, J.E., 2007. Linking lithology and land use to sources of dissolved and particulate organic matter in headwaters of a temperate, passive-margin river system. Geochim. Cosmochim. Acta 71 (17), 4233–4250.
Lynch, L.M., Sutfin, N.A., Fegel, T.S., Boot, C.M., Covino, T.P., Wallenstein, M.D., 2019. River channel connectivity shifts metabolite composition and dissolved organic matter chemistry. Nat. Commun. 10 (1), 459.
Maavara, T., Lauerwald, R., Regnier, P., Van Cappellen, P., 2017. Global perturbation of organic carbon cycling by river damming. Nat. Commun. 8, 15347.
Mahowald, N.M., Randerson, J.T., Lindsay, K., Munoz, E., Doney, S.C., Lawrence, P., Schlunegger, S., Ward, D.S., Lawrence, D., Hoffman, F.M., 2017. Interactions between land use change and carbon cycle feedbacks. Glob. Biogeochem. Cy 31 (1), 96–113.
Maisonneuve, P., Guillemette, F., Lapierre, J.-F., 2022. Biological and photochemical reactivity of dissolved organic matter in a large temperate river. Limnol. Oceanogr. 67 (6), 1388–1401.
Marcé, R., Obrador, B., Morguí, J., Riera, J.L., López, P., Armengol, J., 2015. Carbonate weathering as a driver of CO_2 supersaturation in lakes. Nat. Geosci. 8 (2), 107–111.
Murphy, K.R., Butler, K.D., Spencer, R.G.M., Stedmon, C.A., Boehme, J.R., Aiken, G.R., 2010. Measurement of dissolved organic matter fluorescence in aquatic environments: an interlaboratory comparison. Environ. Sci. Technol. 44 (24), 9405–9412.
Nai, H., Zhong, J., Yi, Y., Lai, M., He, D., Dittmar, T., Liu, C.-Q., Li, S.-L., Xu, S., 2023. Anthropogenic disturbance stimulates the export of dissolved organic carbon to rivers on the tibetan plateau. Environ Sci Technol 57 (25), 9214–9223.
Ni, M., Ge, Q., Li, S., Wang, Z., Wu, Y., 2021. Trophic state index linked to partial pressure of aquatic carbon dioxide in a typical karst plateau lake. Ecol. Indic. 120, 106912.
Ni, M., Li, S., 2023. Ultraviolet humic-like component contributes to riverine dissolved organic matter biodegradation. J. Environ. Sci. 124, 165–175.
Ni, M.F., Li, S.Y., 2022. Dynamics and internal links of dissolved carbon in a karst river system: implications for composition, origin and fate. Water Res. 226, 119289.
Palmer, M., Ruhi, A., 2019. Linkages between flow regime, biota, and ecosystem processes: implications for river restoration. Science 365 (6459), eaaw2087.
Peng, X., Liu, C.-Q., Wang, B., Zhao, Y.-C., 2014. The impact of damming on geochemical behavior of dissolved inorganic carbon in a karst river. Chin. Sci. Bull. 59 (19), 2348–2355.
Ran, L., Butman, D.E., Battin, T.J., Yang, X., Tian, M., Duvert, C., Hartmann, J., Geeraert, N., Liu, S., 2021. Substantial decrease in CO_2 emissions from Chinese inland waters due to global change. Nat. Commun. 12 (1), 1730.
Ran, L., Lu, X.X., Richey, J.E., Sun, H., Han, J., Yu, R., Liao, S., Yi, Q., 2015. Long-term spatial and temporal variation of CO_2 partial pressure in the Yellow River. China. Biogeosci. 12 (4), 921–932.
Ran, L.S., Li, L.Y., Tian, M.Y., Yang, X.K., Yu, R.H., Zhao, J., Wang, L.X., Lu, X.X., 2017. Riverine CO_2 emissions in the Wuding River catchment on the Loess Plateau: environmental controls and dam impoundment impact. J. Geophys. Res. -Biogeosci. 122 (6), 1439–1455.
Raymond, P.A., Hamilton, S.K., 2018. Anthropogenic influences on riverine fluxes of dissolved inorganic carbon to the oceans. Limnol. Oceanogr. Lett. 3 (3), 143–155.
Raymond, P.A., Hartmann, J., Lauerwald, R., Sobek, S., McDonald, C., Hoover, M., Butman, D., Striegl, R., Mayorga, E., Humborg, C., Kortelainen, P., Durr, H., Meybeck, M., Ciais, P., Guth, P., 2013. Global carbon dioxide emissions from inland waters. Nature 503 (7476), 355–359.
Raymond, P.A., Oh, N.-H., Turner, R.E., Broussard, W., 2008. Anthropogenically enhanced fluxes of water and carbon from the Mississippi river. Nature 451 (7177), 449–452.
Regnier, P., Friedlingstein, P., Ciais, P., Mackenzie, F.T., Gruber, N., Janssens, I.A., Laruelle, G.G., Lauerwald, R., Luyssaert, S., Andersson, A.J., Arndt, S., Arnosti, C., Borges, A.V., Dale, A.W., Gallego-Sala, A., Goddéris, Y., Goossens, N., Hartmann, J., Heinze, C., Ilyina, T., Joos, F., LaRowe, D.E., Leifeld, J., Meysman, F.J.R., Munhoven, G., Raymond, P.A., Spahni, R., Suntharalingam, P., Thullner, M., 2013. Anthropogenic perturbation of the carbon fluxes from land to ocean. Nat. Geosci. 6 (8), 597–607.
Sharma, P., Laor, Y., Raviv, M., Medina, S., Saadi, I., Krasnovsky, A., Vager, M., Levy, G. J., Bar-Tal, A., Borisover, M., 2017. Compositional characteristics of organic matter and its water-extractable components across a profile of organically managed soil. Geoderma 286, 73–82.
Song, X., Zhao, Y., Zhang, L., Xie, X., Wu, J., Wei, Z., Yang, H., Zhang, S., Song, C., Jia, L., 2022. Photodegradation, bacterial metabolism, and photosynthesis drive the dissolved organic matter cycle in the Heilongjiang river. Chemosphere 295, 133923.
Spencer, R.G.M., Kellerman, A.M., Podgorski, D.C., Macedo, M.N., Jankowski, K., Nunes, D., Neill, C., 2019. Identifying the molecular signatures of agricultural expansion in amazonian headwater streams. J. Geophys. Res.: Biogeosci. 124 (6), 1637–1650.
Stedmon, C.A., Bro, R., 2008. Characterizing dissolved organic matter fluorescence with parallel factor analysis: a tutorial. Limnol. Oceanogr.: Methods 6 (11), 572–579.
Sun, P.a., He, S., Yu, S., Pu, J., Yuan, Y., Zhang, C., 2021. Dynamics in riverine inorganic and organic carbon based on carbonate weathering coupled with aquatic photosynthesis in a karst catchment, Southwest China. Water Res. 189, 116658.
Tang, X., Woodcock, C.E., Olofsson, P., Hutyra, L.R., 2021. Spatiotemporal assessment of land use/land cover change and associated carbon emissions and uptake in the Mekong River Basin. Remote Sens. Environ. 256, 112336.
Tortell, P.D., Asher, E.C., Ducklow, H.W., Goldman, J.A.L., Dacey, J.W.H., Grzymski, J. J., Young, J.N., Kranz, S.A., Bernard, K.S., Morel, F.M.M., 2014. Metabolic balance of coastal Antarctic waters revealed by autonomous pCO_2 and $\Delta O_2/Ar$ measurements. Geophys. Res. Lett. 41 (19), 6803–6810.
Vilmin, L., Flipo, N., Escoffier, N., Rocher, V., Groleau, A., 2016. Carbon fate in a large temperate human-impacted river system: focus on benthic dynamics. Glob. Biogeochem. Cy. 30 (7), 1086–1104.
Wang, W., Li, S.-L., Zhong, J., Slowinski, S., Li, S., Li, C., Su, J., Yi, Y., Dong, K., Xu, S., Van Cappellen, P., Liu, C.-Q., 2022. Carbonate mineral dissolution and photosynthesis-induced precipitation regulate inorganic carbon cycling along the karst river-reservoir continuum. SW China. J. Hydrol. 615, 128621.
Wang, Y., Zhang, L., Han, X., Zhang, L., Wang, X., Chen, L., 2021. Fluorescent probe for mercury ion imaging analysis: strategies and applications. Chem. Eng. J. 406, 127166.
Williamson, J.L., Tye, A., Lapworth, D.J., Monteith, D., Sanders, R., Mayor, D.J., Barry, C., Bowes, M., Bowes, M., Burden, A., Callaghan, N., Farr, G., Felgate, S., Fitch, A., Gibb, S., Gilbert, P., Hargreaves, G., Keenan, P., Kitidis, V., Juergens, M., Martin, A., Mounteney, I., Nightingale, P.D., Pereira, M.G., Olszewska, J., Pickard, A., Rees, A.P., Spears, B., Stinchcombe, M., White, D., Williams, P., Worrall, F., Evans, C., 2023. Landscape controls on riverine export of dissolved organic carbon from Great Britain. Biogeochemistry 164 (1), 163–184.
Wilson, H.F., Xenopoulos, M.A., 2009. Effects of agricultural land use on the composition of fluvial dissolved organic matter. Nat. Geosci. 2 (1), 37–41.
Wohl, E., Hall Jr, R.O., Lininger, K.B., Sutfin, N.A., Walters, D.M, 2017. Carbon dynamics of river corridors and the effects of human alterations. Ecol. Monogr. 87 (3), 379–409.
Xu, B., Li, J., Huang, Q., Gong, Q., Li, L., 2016. Impacts of land use patterns and typhoon-induced heavy rainfall event on dissolved organic matter properties in the South Tiaoxi river. China. Environ. Earth Sci. 75 (8), 632.
Zhang, J., Li, S., Dong, R., Jiang, C., Ni, M., 2019. Influences of land use metrics at multi-spatial scales on seasonal water quality: a case study of river systems in the Three Gorges Reservoir area. China. J. Clean. Prod. 206, 76–85.
Zhao, M., Liu, Z., Li, H.-C., Zeng, C., Yang, R., Chen, B., Yan, H., 2015. Response of dissolved inorganic carbon (DIC) and δ13CDIC to changes in climate and land cover in SW China karst catchments. Geochim. Cosmochim. Acta 165, 123–136.
Zheng, Y., He, W., Li, B., Hur, J., Guo, H., Li, X., 2020. Refractory humic-like substances: tracking environmental impacts of anthropogenic groundwater recharge. Environ. Sci. Technol. 54 (24), 15778–15788.
Zhong, J., Li, S.-L., Ibarra, D.E., Ding, H., Liu, C.-Q., 2020. Solute production and transport processes in chinese monsoonal rivers: implications for global climate change. Glob. Biogeochem. Cy. 34 (9), e2020GB006541.
Zhong, J., Wallin, M.B., Wang, W., Li, S.-L., Guo, L., Dong, K., Ellam, R.M., Liu, C.-Q., Xu, S., 2021. Synchronous evaporation and aquatic primary production in tropical river networks. Water Res. 200, 117272.
Zhong, J., Wang, L., Caracausi, A., Galy, A., Li, S.-L., Wang, W., Zhang, M., Liu, C.-Q., Liu, G.-M., Xu, S., 2023. Assessing the deep carbon release in an active volcanic field using hydrochemistry, δ13CDIC and Δ14CDIC. J. Geophys. Res.: Biogeosci. 128 (4), e2023JG007435.
Zhou, J., Wang, J.J., Baudon, A., Chow, A.T., 2013. Improved fluorescence excitation-emission matrix regional integration to quantify spectra for fluorescent dissolved organic matter. J. Environ. Qual. 42 (3), 925–930.
Zhou, Y., Yao, X., Zhou, L., Zhao, Z., Wang, X., Jang, K.-S., Tian, W., Zhang, Y., Podgorski, D.C., Spencer, R.G.M., Kothawala, D.N., Jeppesen, E., Wu, F., 2021. How

hydrology and anthropogenic activity influence the molecular composition and export of dissolved organic matter: observations along a large river continuum. Limnol. Oceanogr. 66 (5), 1730–1742.